2018

Plastic hinge relocation in reinforced concrete beams using Cu-Al-Mn SMA bars

S. Pareek
Nihon University, sanjay.pareek@nihon-u.ac.jp

Maged Youssef
youssef@uwo.ca

Mohamed E. Meshaly
Alexandria University

Y. Araki
Nagoya University, yoshikazu.araki@nagoya-u.jp

Plastic Hinge Relocation in Reinforced Concrete Beams using Cu-Al-Mn SMA Bars

S. Pareek [1, *], Y. Suzuki [2], Y. Araki [3], M.A. Youssef [4, **], M. Meshaly[4, 5]

[1]Nihon University, Department of Architecture, College of Engineering, Koriyama, 963-8642, Japan
[2] Osaka City University, Graduate School of Engineering, Osaka, 558-8585, Japan
[3] Nagoya University, Graduate School of Environmental Studies, Nagoya, 464-8603, Japan
[4]Western University, Civil and Environmental Engineering, London, ON, N6A 5B9, Canada
[5] Alexandria University, Structural Engineering Department, Alexandria, Egypt

Abstract

Self-centering earthquake resistant systems have attracted the attention of researchers because of their promising potential in controlling seismic residual drifts, and, therefore, reducing the associated repair costs. The use of Ni-Ti superelastic shape memory alloy (SMA) constitutes a considerable portion of this research. Cu-Al-Mn superelastic SMA has been recently developed to eliminate the high cost of Ni-Ti SMA, as well as, to have better machining characteristics. This paper explores the use of Cu-Al-Mn SMA bars to relocate the plastic hinge in concrete beams through an experimental-numerical study. The cyclic performance of four beams was examined. The first was reinforced with steel bars and the remaining three were reinforced with combination of SMA and steel bars. The location of the SMA bars was different for each of the examined beams. The beams were loaded such that the moment diagram is zero at midspan and maximum at the ends to simulate the expected seismic moments. Results of the experimental-numerical investigation confirmed the recentering capability of the SMA RC beams. Relocating the plastic hinge, by placing the Cu-Al-Mn SMA bars away from the beam ends, improved the strength, rigidity, and energy dissipation.

Keywords: Shape Memory Alloy, Recentering, Cyclic Testing, Plastic Hinge Relocation, Residual Deformations, Energy Dissipation

[*] Associate Professor S. Pareek, Phone: 81-249-56 8747, Email: pareek@arch.ce.nihon-u.ac.jp
[**] Professor M.A. Youssef, Phone: 1-519-661-2111 x88661, Email: youssef@uwo.ca

1. Introduction

Reinforced concrete (RC) structures, designed per current seismic standards, ensure the life safety of the occupants. However, yielding of the steel rebars leads to permanent seismic residual deformations and considerable amount of damage. Following a strong seismic event, retrofitting of such damaged structures might be impractical, which makes demolition the only valid solution.

The use of superelastic shape memory alloys (SMAs), to solve the problem of permanent residual deformations, received the attention of the research community during the last 30 years. Applications of SMA bars in various civil engineering structures have been extensively reported by Janke et al. [1], Song et al. [2], Alam et al. [3], and Ozbulut et al. [4]. The effectiveness of SMA bars as energy dissipating recentering braces and passive control base isolation devices was demonstrated by Dolce et al. [5, 6]. The seismic response of RC bridge columns with SMA reinforcement was studied by Saiidi and Wang [7]. Extensive experimental and analytical research on the use of SMA bars in RC beams, beam–column connections and concrete moment resisting frames was reported [3, 8, 9, 10, 11, 12, 13, 14, 15, 16, 17, 18, 19]. The mentioned studies have focused on the use of Ni–Ti SMA. This alloy is expensive and difficult to machine, which limit its actual implementation in the construction industry [20]. Based on a recent purchase by a Canadian industry partner, 15 mm diameter SMA bar was purchased at about $1250 per meter. The recently developed large diameter Cu–Al–Mn SMA bars overcome these problems [21, 22, 23], where grains much larger than the bar diameter are developed by cyclic heat treatment [24]. The newly developed large diameter SMA bars offer excellent recoverable strain along with superior machinability, and material cost (estimated to be one-fifth of Ni-Ti SMA cost) [23, 24]. The superelasticity of Cu-Al-Mn SMAs exists at temperatures between -40˚C and +60˚C [25]. The self-

centering capability of this new alloy, when used to reinforce RC beams and to form tension braces in a steel frame, was confirmed experimentally by Shrestha et al. [26] and Araki et al. [20].

Similar to Ni-Ti alloy, the modulus of elasticity and energy dissipation of Cu-Al-Mn alloy are lower than those of steel reinforcing bars. To limit the seismic deformations while using Cu-Al-Mn bars, this paper examines relocating the plastic hinge. Details about the conducted experimental and numerical investigations are given in the following sections.

2. Experimental Program

Four-700 mm long concrete beams with a cross section of 100 mm by 150 mm were prepared. The first beam [beam SD] was reinforced with conventional steel rebars. The three remaining beams were reinforced with 100 mm long Cu-Al-Mn SMA bars, as well as steel rebars. 300 mm-long concrete stubs with cross-section dimensions of 200 mm by 250 mm were cast at the ends of the concrete beams to simplify the test setup. Cross sections of the concrete beam and the concrete stubs are given in Fig. 1.

The longitudinal centroids of the 12 mm-diameter SMA bars were positioned at the end of the beam [beam SMA(0D)], 0.5D from the end of the beam [beam SMA(0.5D)], and 1.0D from the end of the beam [beam SMA(1.0D)], where D = 150 mm. The improved machinability of the SMA bars facilitated threading them to a 10-mm diameter. A 40 mm-long threaded coupler was then used to connect the SMA bars to 10 mm steel bars, as shown in Fig. 2. The overlap between the coupler and each of the steel/SMA bars was 20 mm. Tension tests of the SMA bar-coupler-steel bar assembly showed that failure always occurs in the SMA bars. The beam elevations are shown in Fig. 3.

The concrete mix proportions are given in Table 1 and the concrete properties are given in Table 2. The compression and split cylinder tests are conducted per JIS A1132 [27]. The concrete slump, measured per JIS A1101 method [28], was 180 ± 25 mm.

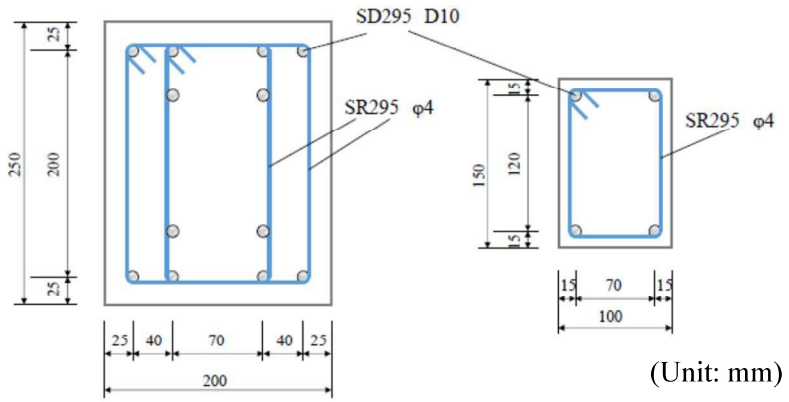

(a) (b)

Fig. 1 Cross-section of (a) Stub, (b) beam

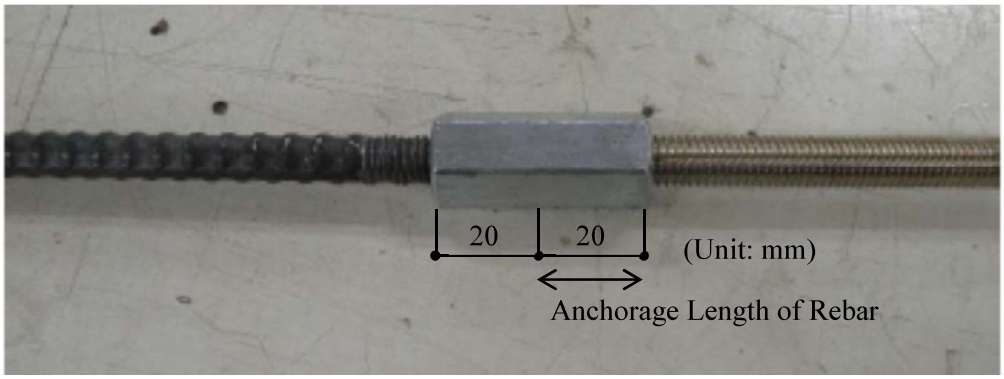

Fig. 2 Steel bar-coupler-SMA bar assembly

Table 1 Mix proportions of concrete

Unit Content (kg/m^3)					S/a (%)	W/C (%)
Cement	Water	Sand	Coarse Aggregate	Admixture		
318	191	821	917	3.18	48	60

Table 2 Concrete properties

Specimen	Compressive strength (MPa)	Compressive strain defining strength	Splitting tensile strength (MPa)
SD	40.1	0.0025	3.47
SMA(0D)	40.4	0.0023	3.31
SMA(0.5D)	34.0	0.0023	2.96
SMA(1.0D)	40.6	0.0024	3.03

Cu-Al-Mn SMA bars having Al content of 17% or less and Mn content of 8% or more were used. The SMA bars were manufactured by hot forging and cold drawing. The martensite-start temperature M_s, the martensite-finish temperature M_f, the austenite-start temperature A_s, and the austenite-finish temperature A_f of the bars were -74˚C, -91˚C, -54˚C, and -39˚C, respectively. The SMA bars were trained using thermal cycling. The experimental stress-strain plots, evaluated by testing only the SMA bars, are shown in Fig. 4. Strains were measured using a non-contact digital video extensometer over a gauge length of 40 mm. Fig. 5 shows a photo of the SMA failure. Properties of the steel and SMA reinforcing bars are given in Table 3. The yield strength and yield strain refer to the point at which SMA structure changes from austenite to martensite.

Table 3 Characteristics of reinforcing bars

Bar	Yield strength (MPa)	Tensile strength (MPa)	Yield strain	Young's Modulus (MPa)
SD295 D10 (steel)	362.9	502.4	0.0019	186,000
M10 (threaded SMA)	179.3	----	0.0073	25,000
	203.9	-----	0.0068	30,000
	201.6	-----	0.0068	30,000
SR295φ4 (steel)	----	560.3	-----	-----

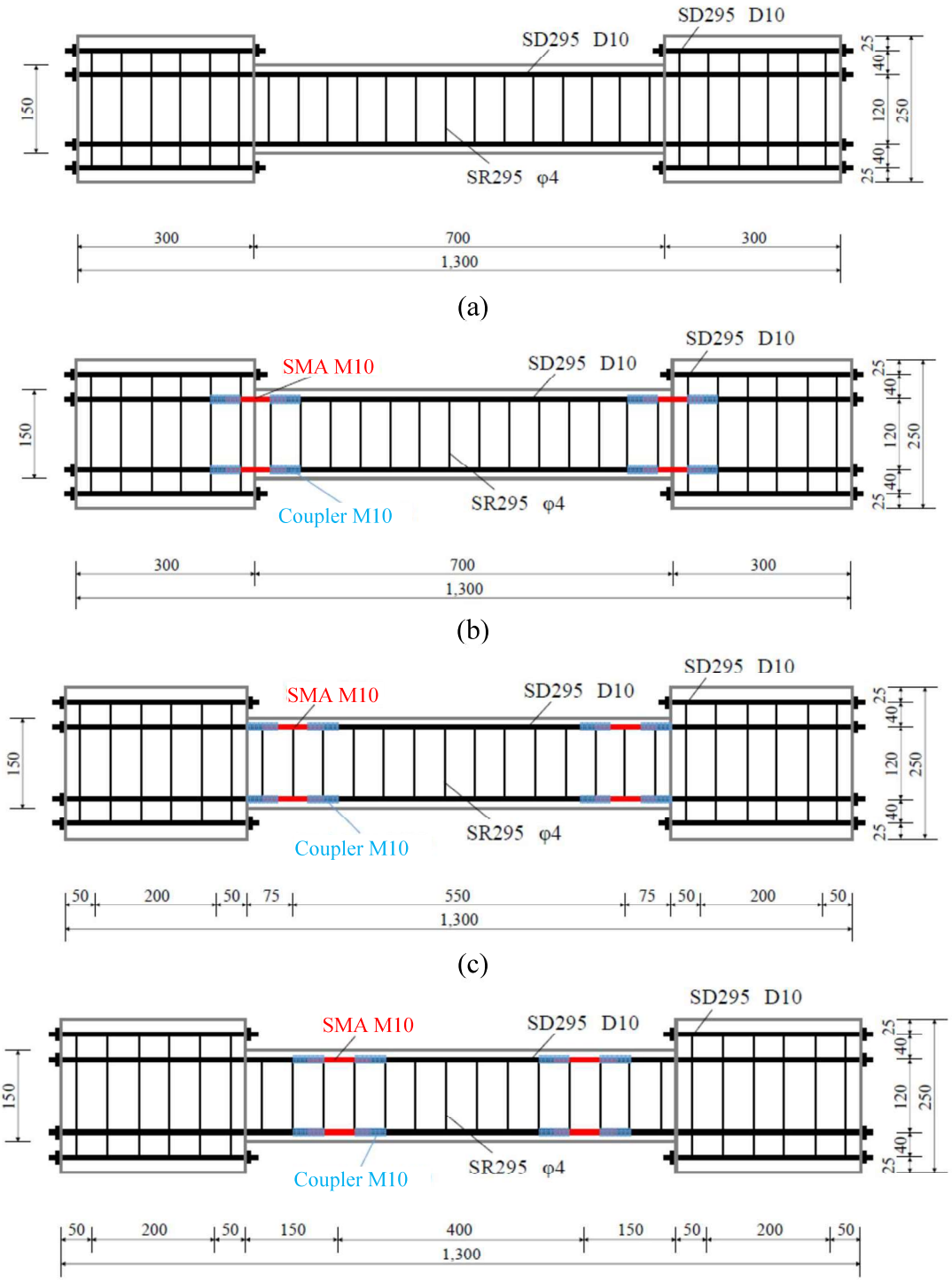

Fig. 3 Elevation of tested specimens. (a) SD, (b) SMA(0D), SMA(0.5D), and (d) SMA(1.0D) (All dimensions in mm)

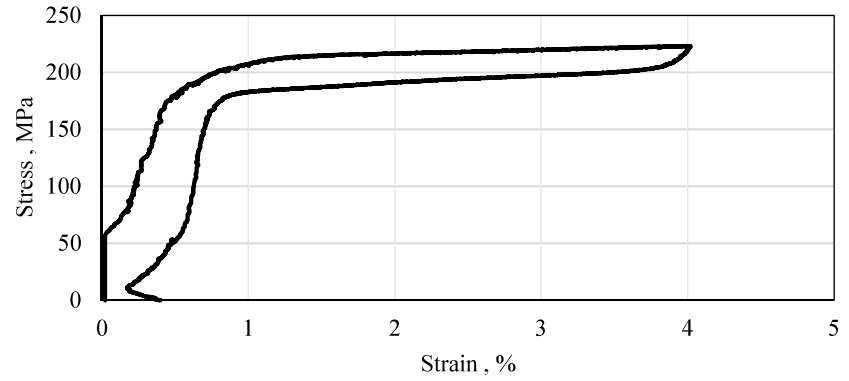

(a)

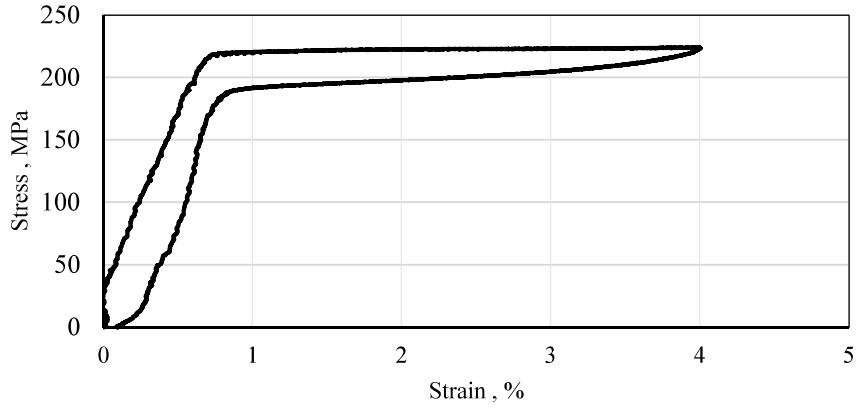

(b)

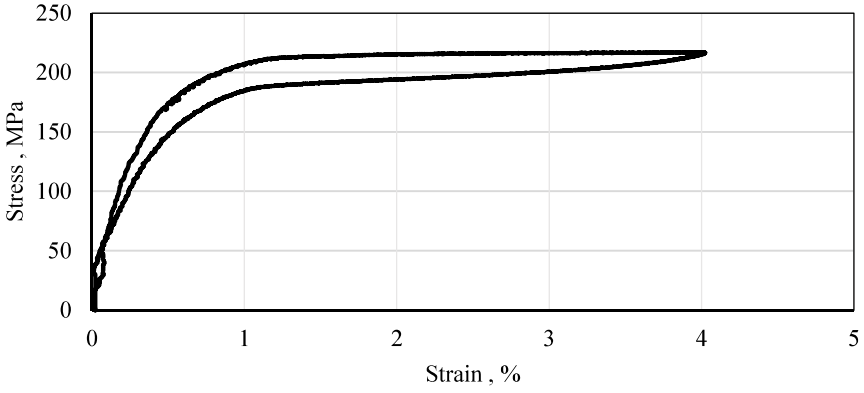

(c)

Fig. 4 Stress-strain plot for SMA bars used in beams (a) SMA(0D), (b) SMA(0.5D), and (c) SMA(1.0D)

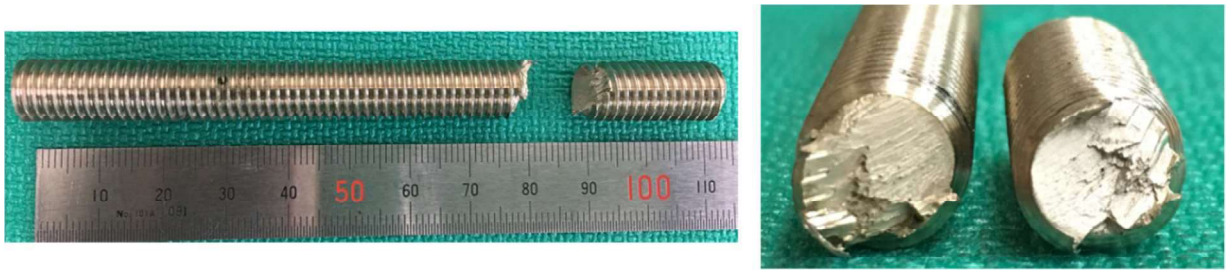

Fig. 5 Typical Tensile Failure of SMA Bars

2.2. Test procedure

To simulate a typical seismic moment diagram, the loads and boundary conditions were set as shown in Fig. 6. The resulting deformation shape is shown in Fig. 7. The length of the stubs and locations of the loads were adjusted to have moments of equal values and opposite signs at the two ends of the beam. Each beam was instrumented with twenty-three displacement gauges as shown in Fig. 8. Gauges 1 to 13 and 14 to 23 were measuring the vertical displacements and the relative axial displacements, respectively. Angles θ_1 and θ_2, shown in Fig. 7a, are evaluated using gauges 1 &3 and 11 & 13, respectively. Using the geometry presented in Fig. 7b, the R value can be evaluated as$(\theta_1 + \theta_2)$. Six cycles of loading were applied such that the beam rotation angle (R) reached values of 0.125%, 0.25%, 0.50%, 1.0%, 1.5%, and 2.0%. As the beam cross section is symmetric, half cycles of loading were applied.

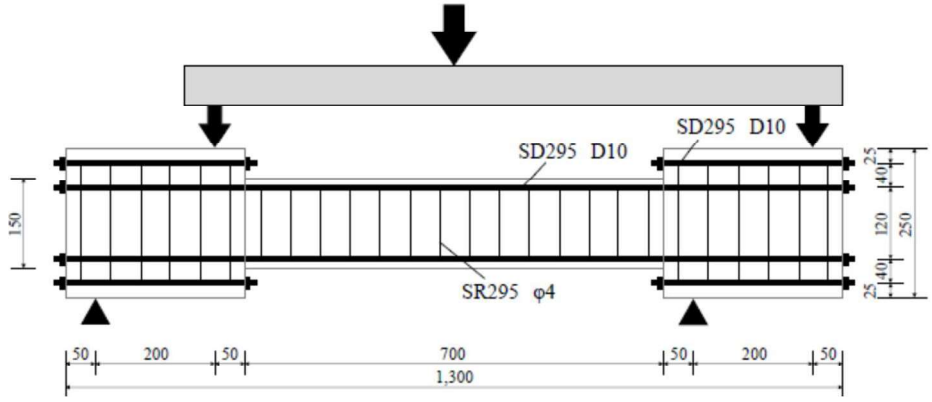

(a)

(b)

Fig. 6 Test setup (a) Schematic, (b) Photo

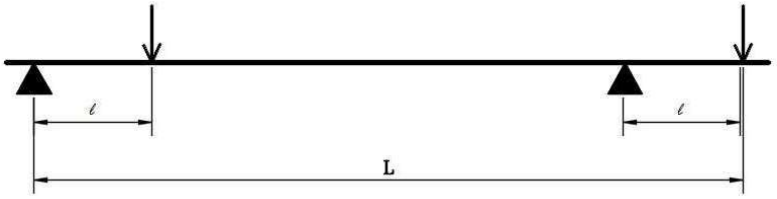

(a)

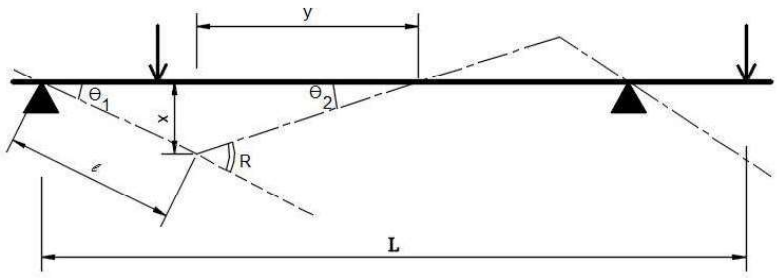

(b)

Fig. 7 Tested specimens (a) Loading, (b) Expected deformation shape

(a)

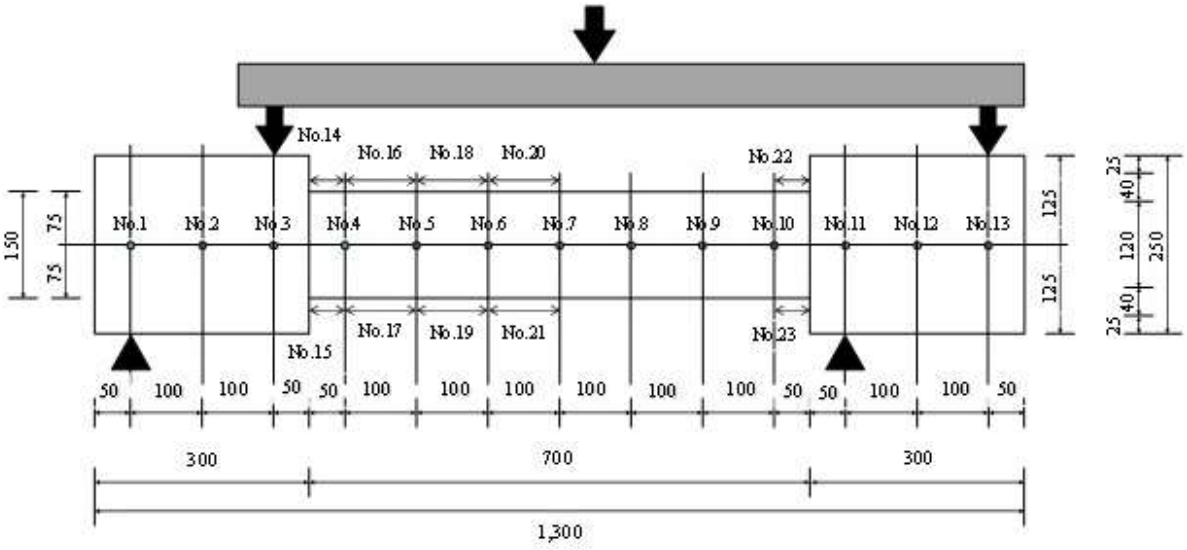

(b)

Fig. 8 Displacement gauges (a) Photo and (b) Locations

3. FE Modeling

FE models were generated using the general-purpose FE program SeismoStruct [29]. Both geometric and material nonlinearities were accounted for. Fiber modeling approach was employed to represent the distribution of material nonlinearity along the beam length and within the cross-sectional area of the member.

Concrete was modeled using the uniaxial nonlinear constant confinement model proposed by Mander et al. [30] and programmed by Madas [31]. The cyclic rules proposed by Martinez-Rueda and Elnashai [32] were adopted. The Menegotto-Pinto model (Menegotto and Pinto [33]), Fig. 9, was employed to account for the hysteretic stress-strain behavior of the steel rebars.

SMA was modeled per the model of Auricchio and Sacco [34], shown in Fig. 10. The parameters used to define the SMA model are: $F_{y(SMA)}$ (austenite to martensite starting stress); f_{P1} (austenite to martensite finishing stress); f_{T1} (martensite to austenite starting stress); f_{T2} (martensite to austenite finishing stress), ε_l (superelastic strain limit); and E_{SMA} (modulus of elasticity).

Slippage between the SMA and steel bars was modeled to account for the observed residual strains that are shown in Fig. 4. These strains are due to material characteristic of the used SMA. A force-displacement spring was used to connect the steel and SMA bars. The modified Takeda hysteresis curve, which is described by Otani [35] and follows the unloading rules of Emori and Schnobrich [36], was utilized to model the force-displacement relationship of the spring element. Five parameters are necessary to characterize the behavior: the yield strength (F_{ys}); the initial stiffness (K_{ys}); ratio of the post-yield stiffness to the initial stiffness (α_s); the outer-loop stiffness degradation factor (b_{0s}); and the inner loop stiffness degradation factor (b_{1s}). The recommended values for the

stiffness degradation factors (b_{0s}=0.1 and b_{1s}=0.9) were specified. A sensitivity analysis was conducted to define the remaining parameters. Values for F_{ys}, K_{ys} and α_s were assumed to be within the ranges given in Table 4. The beams were then analyzed. The best predictions were obtained using the parameters reported in Table 5. SMA properties for specimens SMA(0.5D) and SMA(1.0D) were similar, which led to similar spring properties. Specimen SMA(0D) had slightly different SMA properties, which led to minor difference in the spring properties.

Table 4 Assumed range for each parameter in the sensitivity analysis

Parameter	Assumed values
F_{ys} (N/mm^2)	1,000 to 10,000 with increment of 1,000 10,000 to 100,000 with increment of 10,000
K_{ys} (N/mm)	10^3 to 10^{11} with increment of 10^2
α_s	0.001, 0.01, 0.03, 0.05, 0.07, 0.08, 0.10, 0.15, 0.20, 0.30, and 0.40

Table 5 SMA and spring properties for finite element analysis

Specimen	SMA		Spring Properties		
	E_{SMA} (MPa)	$F_{y(SMA)}$ (MPa)	F_{ys} (N/mm^2)	K_{ys} (N/mm)	α_s
SMA(0D)	25,000	179.3	8,000	100,000	0.07
SMA(0.5D)	30,000	203.9	8,000	100,000	0.08
SMA(1.0D)	30,000	201.6	8,000	100,000	0.08

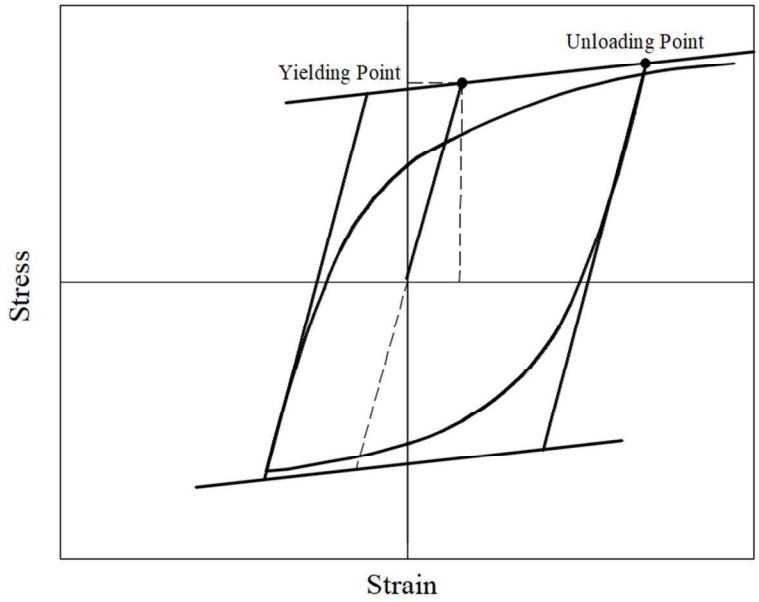

Fig. 9 Steel model

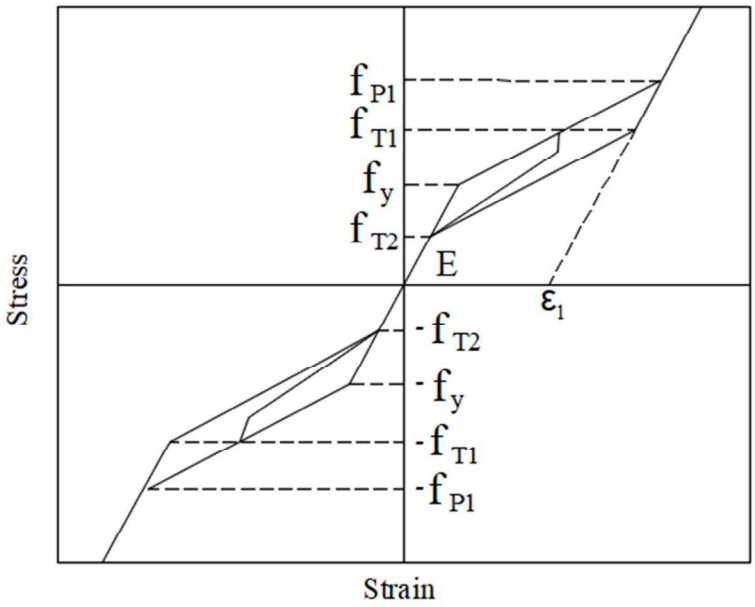

Fig. 10 Superelastic model of SMA

4. Specimen Behaviour

Fig. 11 shows the relationships between the shear force (Q) and the rotation angle (R) for each beam. Both the experimental and finite element results are shown. Predictions of the finite element analysis for the shear strength, energy dissipation, maximum R, and residual R are found to closely match the experimental results. The figure also shows the Q-R relationship as predicted using the design equations of AIJ [37]. Equations (1), (2), and (3) evaluate the moment at cracking (M_c), the yield moment (M_y), and the ultimate moment (M_u), respectively. The corresponding cracking and yield rotations are evaluated based on the elastic stiffness (K) and the reduced yield stiffness ($\alpha_y K$, Equation 4), respectively.

$$M_c = 0.56\sqrt{\sigma_B}Z \qquad (1)$$

$$M_y = a_t \sigma_y \frac{7}{8} d \qquad (2)$$

$$M_u = 0.9 a_t \sigma_y d \qquad (3)$$

$$\alpha_y = (0.043 + 1.64 n p_t + 0.043 a/D) \cdot (d/D)^2 \qquad (4)$$

Where σ_B is the concrete compressive strength [MPa], σ_y is the yield strength of the rebars [MPa], Z is the elastic modulus of the beam section [mm^3], D is the beam height [mm], d is the effective depth of the beam [mm], a_t is the cross-sectional area of the tension rebars [mm^2], p_t is the ratio of the tension rebars to the area of the concrete, n is the modulus ratio, and a is the shear span ratio.

The ultimate rotation is assumed to be 2.0%. AIJ design equations seem to provide a good approximation for the envelope of the experimental Q-R relationship. They have been originally derived based on statistical analysis of numerous experimental results.

The energy dissipation, strength, and residual rotation for specimen SMA(0D) are much lower than those for specimen SD. Moving the SMA bars away from the beam-end has improved the

strength and energy dissipation characteristics. The residual deformations are increased but they are still approximately one-third of the steel reinforced counterpart.

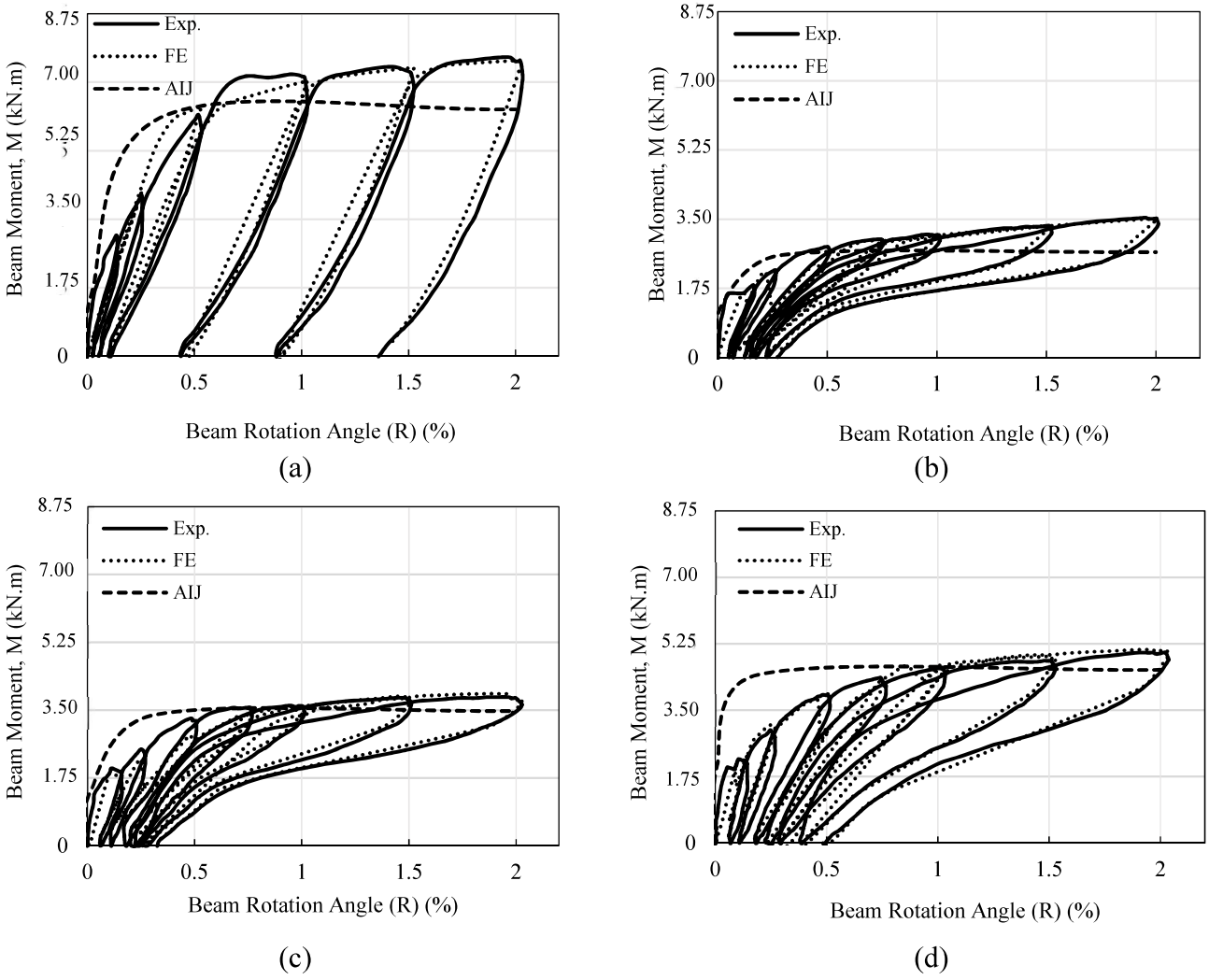

Fig. 11 Relationship between beam shear force and beam rotation angle (a) SD, (b) SMA(0D), (c) SMA(0.5D), (d) SMA(1.0D)

The variation of the curvature at different sections and the crack patterns are shown in Fig. 12. The curvature values give an indication of the location and extent of the plastic hinge. The widest crack for each beam is shown as a heavy line. Finite element results for section A of specimens SD and SMA(0D) and sections A and B for specimens SMA(0.5D) and SMA(1.0D) are also shown. The finite element results are found to agree well with the experimental results. For specimens SD and

SMA(0D), the highest curvature is in region A, that is located near the beam end. Moving the SMA bars away from the beam ends has affected the curvature distribution along the beam length. For specimen SMA(0.5D), the curvature of regions A and B are found to be similar. For specimen SMA(1.0D), the curvature of region B is the highest.

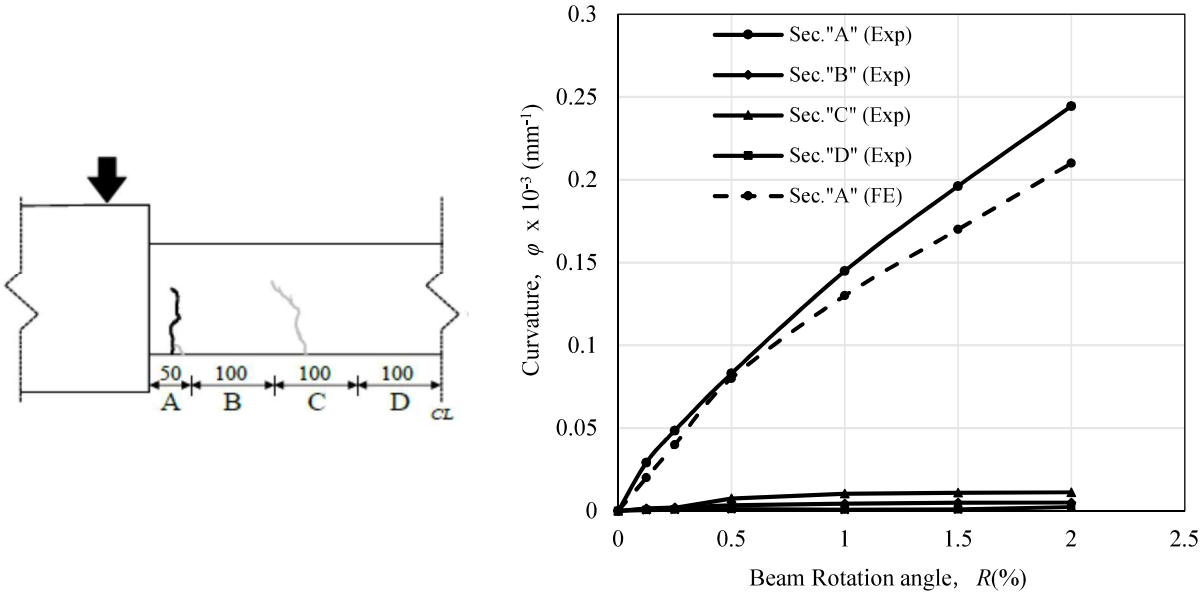

(a)

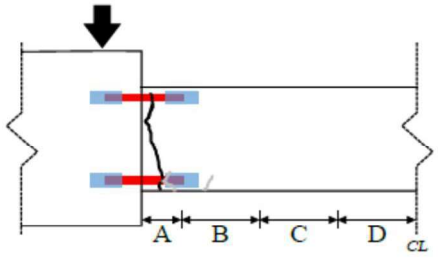
A
B
C
D
CL

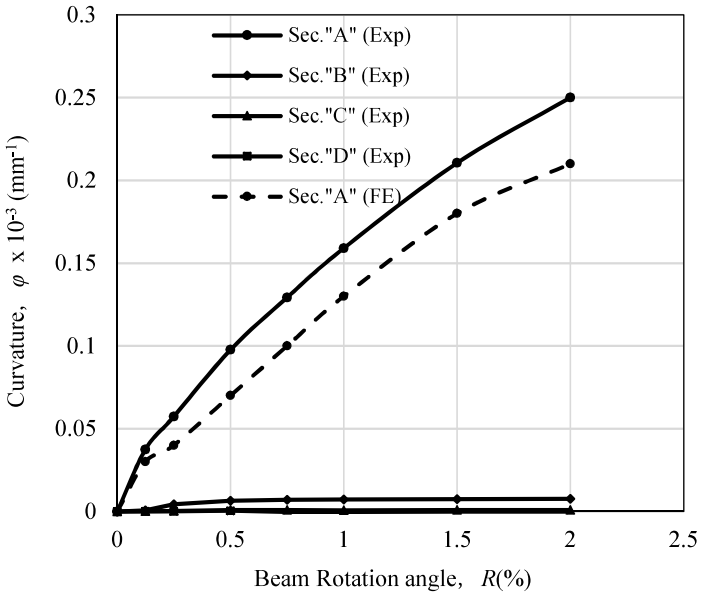
Sec."A" (Exp)
Sec."B" (Exp)
Sec."C" (Exp)
Sec."D" (Exp)
Sec."A" (FE)
Curvature, φ x 10-3 (mm-1)
Beam Rotation angle, R(%)
0.3
0.25
0.2
0.15
0.1
0.05
0
0
0.5
1
1.5
2
2.5

(b)

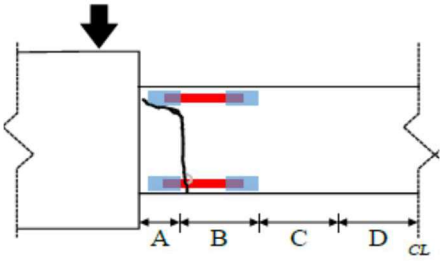
A
B
C
D
CL

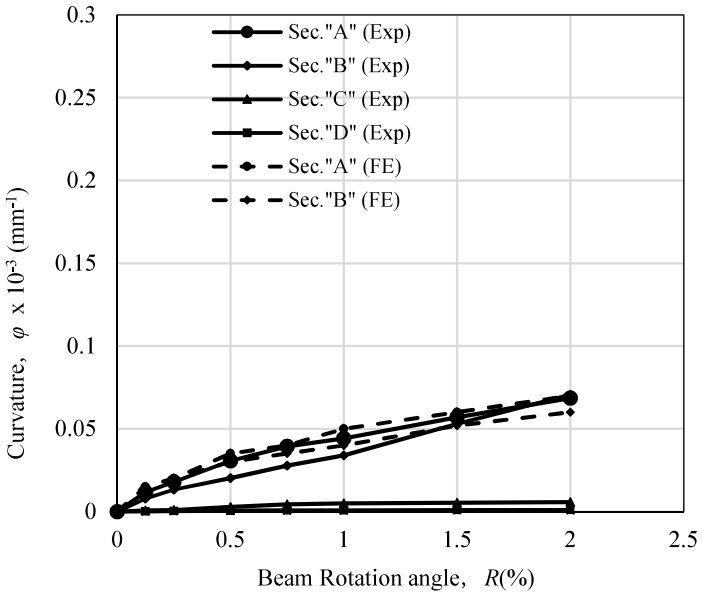
Sec."A" (Exp)
Sec."B" (Exp)
Sec."C" (Exp)
Sec."D" (Exp)
Sec."A" (FE)
Sec."B" (FE)
Curvature, φ x 10-3 (mm-1)
Beam Rotation angle, R(%)
0.3
0.25
0.2
0.15
0.1
0.05
0
0
0.5
1
1.5
2
2.5

(c)

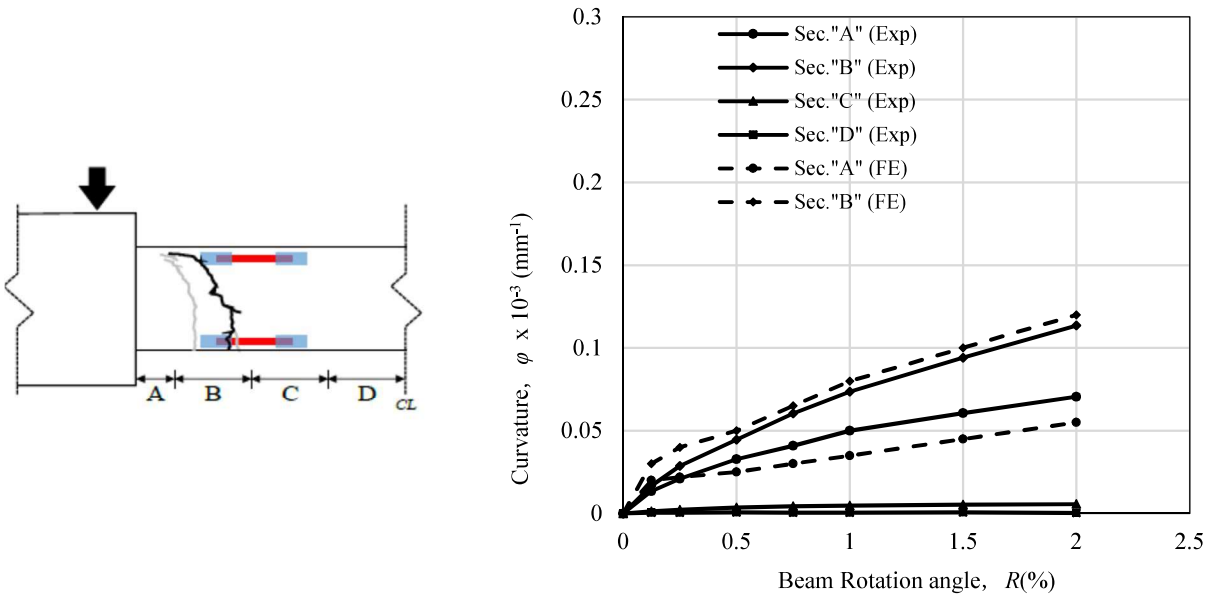

(d)

Fig. 12 The progress of the curvature with respect to rotation angle and the crack pattern at failure (a) SD, (b) SMA(0D), (c) SMA(0.5D), (d) SMA(1.0D)

The variation of the peak and residual crack width for each specimen is shown in Fig. 13. For the SD specimen at R of 2.0%, the residual crack width exceeds 0.3 mm. For specimens SMA(0D), SMA(0.5D), and SMA(1.0D), the residual crack width does not exceed 0.3 mm, due to the deformation recovery of the superelastic alloy. However, cracks have initiated at an earlier stage than the SD specimen. This might be due to the lower rigidity and strength of the SMA specimen. The hinge relocation has improved the rigidity of specimen SMA(0.5D).

From Fig. 11, it is clear that the energy dissipation of the SD specimen is almost constant for cycles reaching rotation angles of 1.0%, 1.5%, and 2.0%. The SMA specimens have behaved in a different way due to their deformation recovery. Their cumulative energy has increased with the increase of R. Fig. 14 shows an initial sharp decline in the cumulative energy dissipation of the SMA

specimens as compared to the SD specimen. This decline continued until reaching an R value of about 1%, where the relationship has changed to a slight increase in the energy dissipation of the SMA specimens. Locating SMA bars away from the beam ends increases the energy dissipation due to reaching higher moment values.

Fig. 15 shows variation of rigidity, normalized using the first cycle of loading, with the rotation. Comparing the SD and SMA(0D) specimens, the difference in the rate of decrease is about 20% at R of 0.5%. This difference is reduced to about 10% for specimen SMA(1.0D), due to the higher contribution of the unyielded steel bars on the rigidity of the beam.

Fig. 16 shows the variation of the secant rigidity of the SMA specimens, measured at the peak load and normalized using the secant rigidity of the SD specimen, with the rotation. Although, there are no significant changes in the relative secant rigidity, its value is different for each specimen. Moving the SMA bars away from the beam ends is found to increase the secant rigidity.

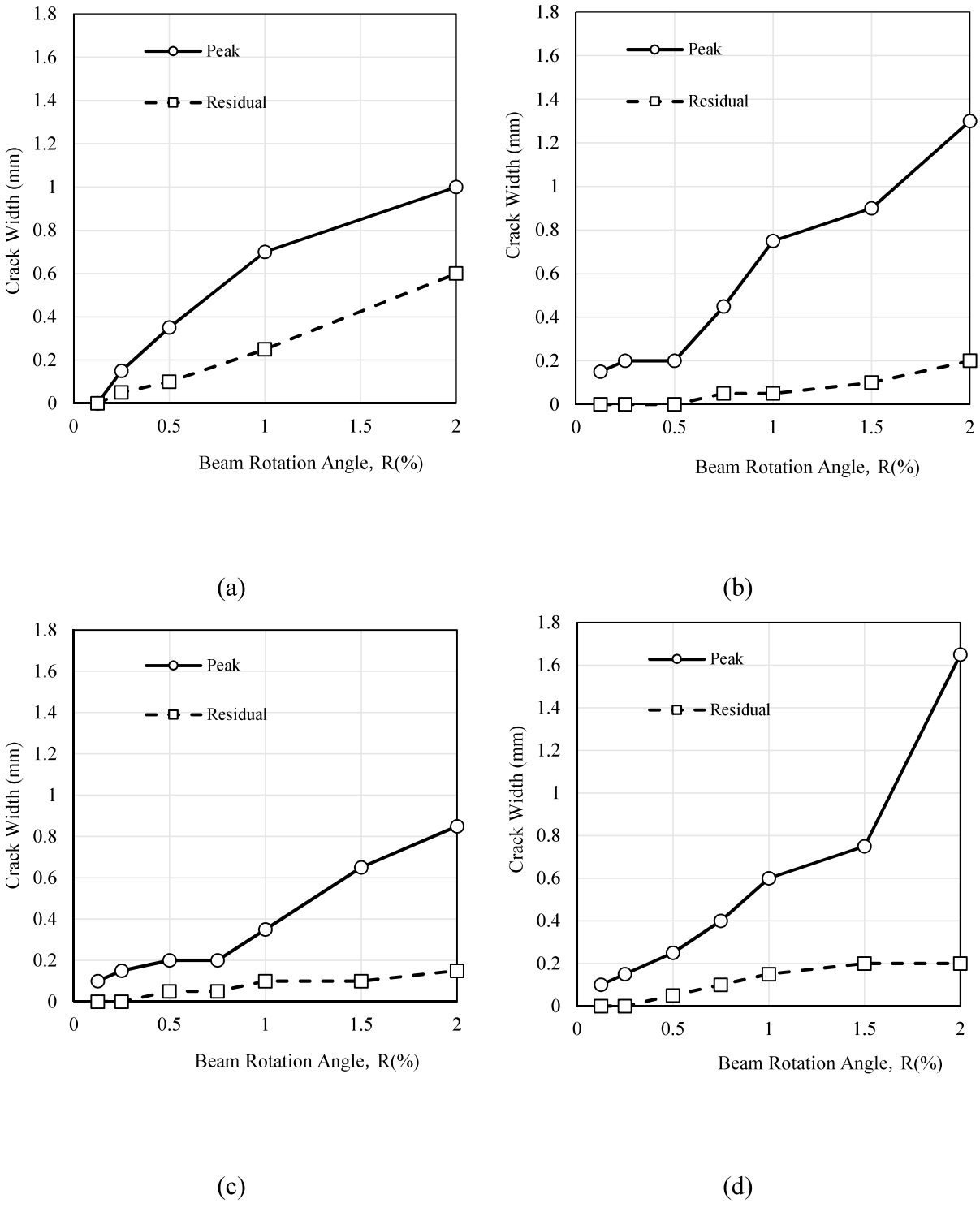

Fig. 13 Relationship between crack width and beam rotation angle (a) SD, (b) SMA(0D), (c) SMA(0.5D), (d) SMA(1.0D)

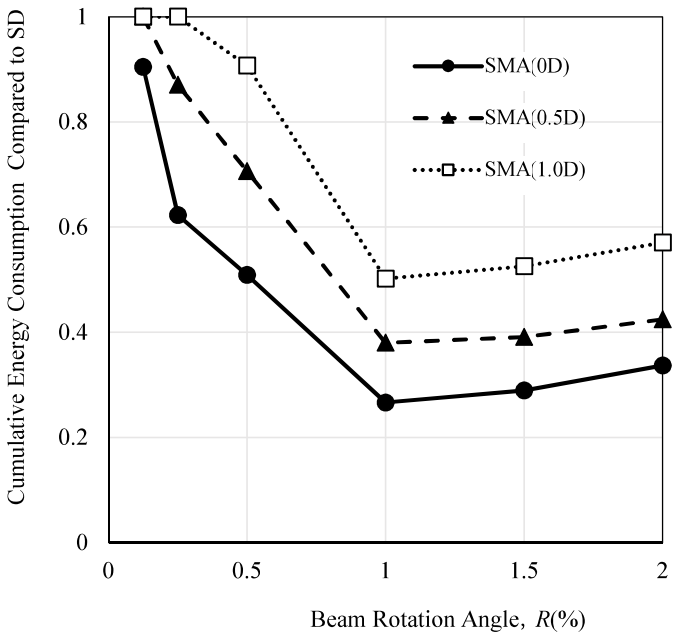

Fig. 14 Relationship between the beam rotation angle (R) and the cumulative energy dissipation of the SMA specimens as compared to the SD specimen

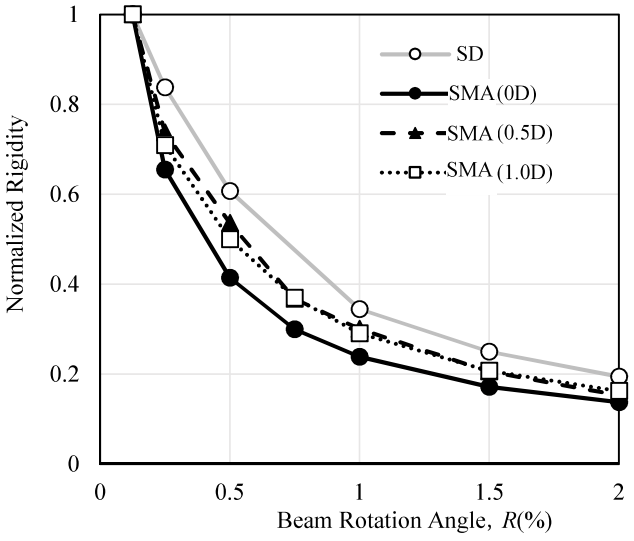

Fig. 15 Relationship between the rigidity and the beam rotation angle

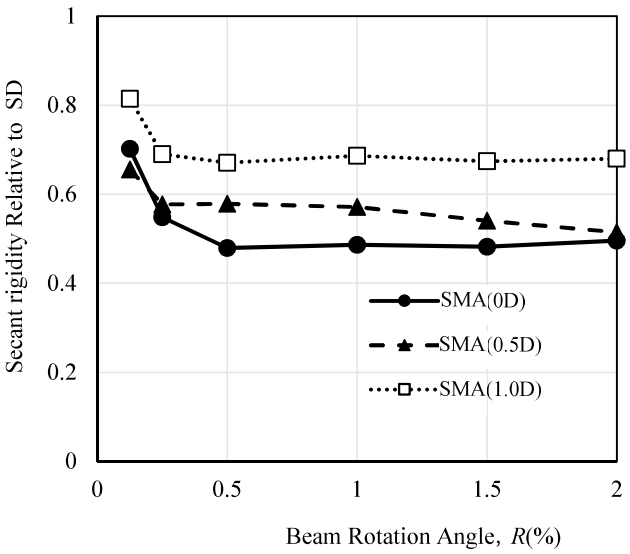

Fig. 16 Secant rigidity at the peak load of SMA specimens relative to the SD specimen

5. Conclusions

In this paper, an experimental-numerical study is conducted to explore the cyclic behaviour of RC beams, partially reinforced with a newly developed superelastic SMA. The study has explored relocating the plastic hinge by moving the SMA bars away from the beam end.

The experimental results have confirmed the ability of the new alloy to significantly reduce the residual displacements. Replacing steel bars with SMA bars, at the beam ends, have lowered the strength, energy dissipation, and residual deformations. The undesirable reduction in strength and energy dissipation can be improved by relocating the plastic hinge, which slightly affects the improvement in residual deformations. Moving the SMA bars away from the beam ends has changed the curvature distribution along the beam length. The highest curvature value is measured at the location of the SMA bars, because of their relatively low yield strength. In this case, the deformation concentrates at the location of the SMA bars, which have increased the overall strength of the beam and have resulted in higher energy dissipation.

The strength and rigidity of the RC beams, after relocating the plastic hinge using SMA bars, have been reasonably predicted using AIJ design equations. Finite element models have been generated to simulate the experiments. A sensitivity analysis is conducted to model the observed residual strains in the tension tests of the steel-coupler-SMA assembly. Results from this analysis have led to defining the parameters for the force-displacement spring that joins the SMA bars and the steel bars. The use of such a spring in the finite element model has led to excellent analytical predictions that are closely matching the experimental studies. For future analytical studies, the parameters defining this spring might require calibration based on the dimensions of the examined beams.

Acknowledgments

Funding for this research was provided by the Japanese Scientific Research / Basic Research (A) (Number: 16H02376) and (C) (Number: 16K06590), and the Natural Sciences and Engineering Research Council of Canada (NSERC). The SMA bars were produced by Furukawa Techno Materials Special Metals under the supervision of Mr. Sumio Kise.

6. References

1. Janke L., Czaderski C., Motavalli M., and Ruth J. "Applications of Shape Memory Alloys in Civil Engineering Structures-Overview, Limits and New Ideas." Materials and Structures 38, no. 5 (2005): 578–92.

2. Song, G., Ma N., and Li H.N. "Applications of Shape Memory Alloys in Civil Structures." Engineering Structures 28, no. 9 (2006a): 1266–74.

3. Alam M., Nehdi M., and Youssef M.A., "Seismic Performance of Concrete Frames Reinforced with Superelastic Shape Memory Alloys." Smart Structures and Systems 5, no.5 (2009): 565–85.

4. Ozbulut O.E., Hurlebaus S., and Desroches R. "Seismic Response Control Using Shape Memory Alloys: A Review." Journal of Intelligent Material Systems and Structures 22, no. 14 (2011): 1531–49.

5. Dolce M., Cardone D., Ponzo F.C., and Valente C. "Shaking Table Tests on Reinforced Concrete Frames without and with Passive Control Systems." Earthquake Engineering & Structural Dynamics 34, no. 14 (2005): 1687–1717.

6. Dolce M., Cardone D., and Ponzo F.C. "Shaking-Table Tests on Reinforced Concrete Frames with Different Isolation Systems." Earthquake Engineering & Structural Dynamics 36, no. 5 (2007): 573–96.

7. Saiidi, M. S., and Wang H. "Exploratory Study of Seismic Response of Concrete Columns with Shape Memory Alloys Reinforcement." Structural Journal 103, no. 3 (2006): 435–42.

8. Abdulridha A., Palermo D., Foo S., Vecchio F. "Behavior and modeling of superelastic shape memory alloy reinforced concrete beams." Engineering Structures. 49 (2013): 893–904.

9. Deng Z., Li Q., and Sun H. "Behavior of Concrete Beam with Embedded Shape Memory Alloy Wires." Engineering Structures 28, no. 12 (2006): 1691–97.

10. Song G., Mo Y.L., Otero K., and Gu H. "Health Monitoring and Rehabilitation of a Concrete Structure Using Intelligent Materials." Smart Materials and Structures 15, no. 2 (2006b): 309-14.

11. Li H., Liu Z., and Ou J. “Study on Reinforced Concrete Beams Strengthened Using Shape Memory Alloy Wires in Combination with Carbon-Fiber-Reinforced Polymer Plates.” Smart Materials and Structures 16, no. 6 (2007): 2550.

12. Kuang Y., and Ou J. “Self-Repairing Performance of Concrete Beams Strengthened Using Superelastic SMA Wires in Combination with Adhesives Released from Hollow Fibers.” Smart Materials and Structures 17, no. 2 (2008): 025020.

13. Youssef M.A., Alam M.S., and Nehdi M. “Experimental Investigation on the Seismic Behavior of Beam-Column Joints Reinforced with Superelastic Shape Memory Alloys.” Journal of Earthquake Engineering 12, no. 7 (2008): 1205–22.

14. Wierschem N., and Andrawes B. “Superelastic SMA–FRP Composite Reinforcement for Concrete Structures.” Smart Materials and Structures 19, no. 2 (2010): 025011.

15. Speicher M.S., Desroches R., and Leon R.T. “Experimental Results of a NiTi Shape Memory Alloy (SMA)-Based Recentering Beam-Column Connection.” Engineering Structures 33, no. 9 (2011): 2448–57.

16. Choi E., Chung Y., Kim Y., and Kim J. “Monotonic and Cyclic Bond Behavior of Confined Concrete Using Ni Ti Nb SMA Wires.” Smart Materials and Structures 20, no. 7 (2011): 075016.

17. Zafar A., and Andrawes B. “Incremental Dynamic Analysis of Concrete Moment Resisting Frames Reinforced with Shape Memory Composite Bars.” Smart Materials and Structures 21, no. 2 (2012): 025013.

18. Youssef M.A., and Elfeki M. “Seismic Performance of Concrete Frames Reinforced with Superelastic Shape Memory Alloys.” Smart Structures and Systems 9, no. 4 (2012): 313–33.

19. Meshaly M., Youssef M.A., and Abou-Elfath H. “Use of SMA Bars to Enhance the Seismic Performance of SMA Braced RC Frames.” Earthquakes and Structures 6, no. 3 (2014): 267–80.

20. Araki Y., Shrestha K., Maekawa N., Koetaka Y., Omori T., and Kainuma R. “Shaking Table Tests of Steel Frame with Superelastic Cu–Al–Mn SMA Tension Braces.” Earthquake Engineering & Structural Dynamics 45, no. 2 (2016): 297–314.

21. Sutou Y., Omori T., Wang J.J., Kainuma R., and Ishida K. “Effect of Grain Size and Texture on Superelasticity of Cu-AI-Mn-Based Shape Memory Alloys.” Journal de Physique IV (Proceedings) 112 (2003): 511–14.

22. Sutou Y., Omori T., Yamauchi K., Ono N., Kainuma R., and Ishida K. “Effect of Grain Size and Texture on Pseudoelasticity in Cu–Al–Mn-Based Shape Memory Wire.” Acta Materialia 53, no. 15 (2005): 4121–33.

23. Araki Y., Endo T., Omori T., Sutou Y., Koetaka Y., Kainuma R., and Ishida K. “Potential of Superelastic Cu–Al–Mn Alloy Bars for Seismic Applications.” Earthquake Engineering & Structural Dynamics 40, no. 1 (2011): 107–15.

24. Omori T, Kusama T, Kawata S, Ohnuma I, Sutou Y, Araki Y, Ishida K, Kainuma R. Abnormal grain growth induced by cyclic heat treatment. Science 2013; 341(6153):1500–1502.

25. Sutou Y., Koeda N., Omori T., Kainuma R., and Ishida K. “Effects of Aging on Stress-Induced Martensitic Transformation in Ductile Cu–Al–Mn-Based Shape Memory Alloys.” Acta Materialia 57, no. 19 (2009): 5759–70.

26. Shrestha, K., Araki Y., Nagae T., Koetaka Y., Suzuki Y., Omori T., Sutou Y., Kainuma R., and Ishida K. “Feasibility of Cu–Al–Mn Superelastic Alloy Bars as Reinforcement Elements in Concrete Beams.” Smart Materials and Structures 22, no. 2 (2013): 025025.

27. Japanese Industrial Standard (2014) JIS standard. Method of Making and Curing Concrete Specimens. JIS A-1132.

28.Japanese Industrial Standard (2014) JIS standard. Method of Test for Slump of Concrete. JIS A-1101.

29. SeismoSoft “Seismostruct: A computer program for static and dynamic nonlinear analysis of framed structures”, (2009) Available from URL: http://www.seismosoft.com/SeismoStruct/index.htm

30. Mander J., Priestley N., and Park R. “Theoretical Stress-Strain Model for Confined Concrete.” Journal of Structural Engineering 114, no. 8 (1988): 1804–26.

31. Madas P. "Advanced Modelling of Composite Frames Subjected to Earthquake Loading." PhD Thesis, Imperial College, University of London, London, UK (1993).

32. Martínez-Rueda J., and Elnashai A. S. “Confined Concrete Model under Cyclic Load.” Materials and Structures 30, no. 3 (1997): 139–47.

33. Menegotto M., Pinto P.E. "Method of analysis for cyclically loaded R.C. plane frames including changes in geometry and non-elastic behaviour of elements under combined normal force and bending." Symposium on the Resistance and Ultimate Deformability of Structures Acted on by Well Defined Repeated Loads, International Association for Bridge and Structural Engineering, Zurich, Switzerland, (1973): 15-22.

34. Auricchio F., and Sacco E. “A Superelastic Shape-Memory-Alloy Beam Model.” Journal of Intelligent Material Systems and Structures 8, no. 6 (1997): 489–501.

35. Otani S. “SAKE, A Computer Program for Inelastic Response of R/C Frames to Earthquakes”, Report UILU-Eng-74-2029, Civil Engineering Studies, University of Illinois at Urbana-Champaign, USA (1974).

36. Emori K., Schnobrich W.C. “Analysis of Reinforced Concrete Frame-Wall Structures for Strong Motion Earthquakes”. Structural Research Series No. 434, Civil Engineering Studies, University of Illinois at Urbana-Champaign (1978).

37. AIJ, “Standards for Structural Calculation of Steel Reinforced Concrete Structures”, Architectural Institute of Japan, Tokyo, Japan (2010).